

Mathematical modelling and simulation of multiphase flow in a flat plate solar energy collector



H.U. Helvaci*, Z.A. Khan

Bournemouth University, Sustainable Design Research Centre (SDRC), Faculty of Science and Technology, Bournemouth BH12 5BB, UK

ARTICLE INFO

Article history:

Received 26 May 2015

Accepted 10 September 2015

Available online 26 September 2015

Keywords:

Flat plate collector

Simulation

Multiphase flow

Heat transfer coefficient

ABSTRACT

Non-conventional collectors where organic fluid or refrigerant experience a phase change have many advantages over conventional collectors which have either air or relatively high temperature boiling liquid. Increase in heat transfer coefficient and system efficiency, corrosion prevention and freeze protection are the main benefits of the first type. In this study, a detailed numerical model of a flat plate collector is developed to investigate the fluid mean temperature, useful heat gain and heat transfer coefficient along the collector tube. The refrigerant HFC-134a was used in the simulation as the working fluid of the collector. The model can both predict the location where the fluid undergoes a phase change in the tube and the state at the exit under given inlet conditions. The effect of boiling on the heat transfer coefficient of the fluid is also investigated. Simulations were performed at three different mass flow rates (0.001, 0.005 and 0.01 kg/s) and three different operating pressures (4, 6 and 8 bar) to be able to see the effect of mass flow rate and pressure on plate temperature, heat loss coefficient, efficiency of the collector and the heat transfer coefficient of the fluid. The simulation results indicate that the heat transfer coefficient of the fluid increases from 153.54 W/m² K to 610.27 W/m² K in multiphase flow region. In the liquid single phase region, the collector efficiency rises from 60.2% to 68.8% and the heat transfer coefficient of the fluid increases from 39.24 W/m² K to 392.31 W/m² K with an increased flow rate whereas the collector efficiency decreases from 72.5% to 62.3% as the operating pressure increases from 4 bar to 8 bar. In order to validate the simulation model an experimental test rig was built and the experiments were performed with HFE 7000 as working thermo-fluid. A new simulation model utilizing HFE 7000 has been developed and the outlet temperature of the fluid was compared with the measured outlet temperature. Both measured and simulated results have shown close conformity.

© 2015 The Authors. Published by Elsevier Ltd. This is an open access article under the CC BY license (<http://creativecommons.org/licenses/by/4.0/>).

1. Introduction

Utilization of fossil fuels has caused many problems such as the release of CO₂ to the atmosphere and its subsequent effects on our environment. This can be changed if our dependence is decreased on fossil fuels by using alternative renewable energy sources [1]. Due to its lower impacts on environment solar energy can be considered as one of the most favourable option to contribute to the energy demand with extensive applications in industry [2]. There has been an upward trend in various kinds of solar energy harvesting systems. A dynamic model of a solar pond was developed in order to investigate the effect of the sunny area ratios on the efficiency by [3]. Experimental and simulation studies on the thermal performance of a room heated with an attached sunspace were

conducted by [4]. The thermal behaviour of volumetric solar receiver with double-layer of porous media and the effects of geometry of each layer on the performance was numerically studied by [5]. Dehghan et al. [6] analysed the effect of radiation heat transfer on forced convective heat transfer mechanism through cellular porous media confined by two parallel plates. The plates subjected to constant heat flux and the Darcy–Brinkman equation was utilized to model the flow through the porous medium [6]. In another study the effects of thermal radiation on the forced convection through cellular porous media considering a combined conductive–convective–radiation heat transfer model were studied by [7].

Solar collectors which convert solar energy into heat produce either hot water or air depending on the working fluid of the collector [8]. Recently, many studies have focused on increasing the efficiency of solar water heaters. An experimental study to investigate the effect of using a mixture of ethylene glycol and copper nanoparticles as a working fluid on the collector efficiency was conducted by [9]. In another study it is reported that using

* Corresponding author at: Faculty of Science and Technology, Fern Barrow, Talbot Campus, Bournemouth University, Poole, Dorset BH12 5BB, UK. Tel.: +44 7473 770009.

E-mail address: hhelvaci@bournemouth.ac.uk (H.U. Helvaci).

Furthermore, various studies have been conducted to analyse solar collectors theoretically where the fluid undergoes a phase change.

An extended mathematical model of a boiling flat plate collector in which fluid and plate temperatures, heat transfer coefficient and vapour quality can be predicted along the collector tube was developed by [11]. Various organic fluids (R-113, n-pentane, methanol, acetone, diethyl ether) and water as a working fluid were used and the effect of transition from single phase flow to the boiling flow was taken into account in the study [11]. Results showed that no matter what working fluid was used, a higher thermal efficiency was obtained in a boiling flow as compared to single phase flow in the collector. Analysis of the boiling collector was studied by [12] where operating characteristics of condenser were also considered in their analysis. The refrigerant R-11 was utilized in a two-phase collector which operates in a thermo syphon mode. TRNSYS simulation program was used for modelling the boiling collector-condenser system which also accounted for heat losses and pressure drops in the vapour and liquid line [12].

Aziz et al. [22], conducted a numerical analysis of a solar collector which was employed as an evaporator of a heat pump cycle. In order to evaluate the size of a solar collector multiphase flow of (R-123–R134a) mixture is analysed, thermodynamic and heat transfer characteristics were calculated. The effect of various mass flow rate of the mixture, solar radiation and inlet pressure on the heat transfer coefficient and collector tube length was also taken into account. Authors concluded that both mass flow rate and solar radiation have important effects on the collector size and heat transfer coefficient of the mixture where operating pressure does not have any significant effect on the tube length of collector [22].

R134a is a hydrofluorocarbon (HFC) refrigerant and has been of interest to Sustainable Design Research Centre (SDRC), Bournemouth University in terms of industrial applications [23,24].

In this study, a detailed numerical model of a flat plate collector is developed to investigate mean temperature, useful heat gain and heat transfer coefficient of HFC-134a along the collector tube. The model can predict both the location where the fluid undergoes a phase change in the tube and the fluid exit state. The effect of mass flow rate of the fluid and operating pressure on the collector efficiency, outlet fluid temperature, absorber plate temperature and heat transfer coefficient of the fluid is also investigated. Furthermore, the model was utilized with novel-thermo fluid (HFE 7000) in order to compare the collector performance between two working fluids. Also, simulation results using HFE 7000 was validated against experimental results.

2. Collector specifications

Serpentine type flat plate collector was used to conduct this simulation and it consists of a cover, absorber, copper tube and insulation at the backend and edges of the collector. Cover (1) with 3 mm thick is used for reducing both radiation and convection loss from the collector. Absorber (2) is a coated stainless steel sheet, of which surface has dark-coloured paint for high absorption property. The thickness of the absorber plate is 1 mm. The fluid is circulated in the copper tubes (3) where the heat is gained from the absorber to the fluid. Conduction loss from the backend and edges of the collector is reduced by insulation (4). The schematic description of the collector is shown in Fig. 1.

3. Mathematical modelling

Developed analytical model of serpentine flat plate collector under a phase change is based on the model represented by [25]. The model is modified and used under following assumptions:

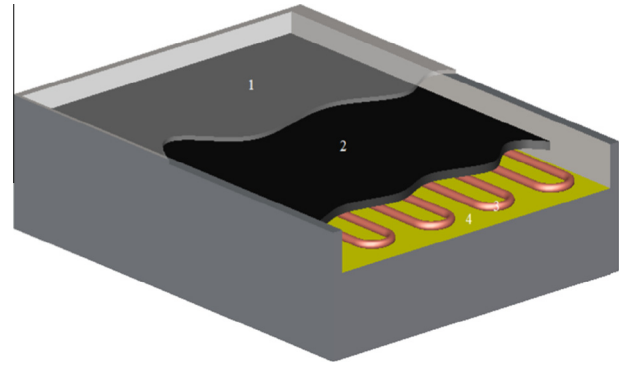


Fig. 1. Schematic of serpentine tube flat plate collector.

- Steady-state conditions.
- Absorber and glass cover thermal and radiation properties are constant (independent of temperature).
- Uniform heat flux conditions are granted instead of uniform wall temperature.
- Entry regions effects are neglected ($L_{\text{tube}}/D = 7000$).
- The fluid undergoes a phase-change as the average fluid temperature reaches the boiling temperature of the fluid at corresponding pressure.
- Both single and multiphase heat transfer coefficient of the fluid varies along the tube.
- Serpentine tube considered as one flat tube to calculate heat transfer coefficients for both single and multiphase flows.

3.1. Heat loss calculation

There are mainly two types of losses occur in a flat plate collector which are optical and thermal losses, respectively. Optical losses can be shown as $S_{\text{in}} (\tau\alpha)$, where $(\tau\alpha)$ is the transmittance-absorbance of the glass cover depending on the material properties. Thermal losses can be divided into three parts which are heat loss from the top of the collector U_{top} , from the back U_{back} and the edge of the collector U_{edge} respectively. During the calculations heat loss through the edges has been ignored. Heat loss from the top of the collector can take place by means of radiation and convection heat transfer mechanism from the glass cover to the atmosphere and from the absorber plate to the cover. Klein [26] generalized formula to calculate the top heat loss coefficient which is shown in Eq. (1).

$$U_{\text{top}} = \left(\frac{N_c}{\frac{C}{T_p} \left[\frac{T_p - T_a}{N_c + f} \right]^e + \frac{1}{h_w}} \right)^{-1} + \frac{\sigma (T_p + T_a) (T_p^2 + T_a^2)}{(\epsilon_p + 0.00591 N_c h_w)^{-1} + \frac{2N_c + f - 1 + 0.133\epsilon_p}{\epsilon_c} - N_c} \quad (1)$$

where

$$f = (1 + 0.0889h_w - 0.1166h_w\epsilon_p)(1 + 0.07866N_c)$$

$$C = 520(1 - 0.000051\beta^2) \text{ for } 0^\circ < \beta < 70^\circ \text{ and if } 70^\circ < \beta < 90^\circ \text{ apply } \beta = 70^\circ$$

$$e = 0.430(1 - 100/T_p)$$

Heat losses from the back of the collector is

$$U_{\text{back}} = \frac{k_{\text{ins}}}{L_{\text{ins}}} \quad (2)$$

Therefore, total heat loss coefficient of the collector becomes

$$U_T = U_{\text{top}} + U_{\text{back}} \quad (3)$$

Absorbed solar energy on the surface of the plate can be written as

$$Q_p = A_p S_{\text{in}}(\tau\alpha) - Q_l \quad (4)$$

When plate temperature (T_p) and heat loss coefficient (U_T) are taken into account, then the absorbed solar energy on the plate surface can be calculated as;

$$Q_p = A_p [S_{\text{in}}(\tau\alpha) - U_T(T_p - T_a)] \quad (5)$$

3.2. Convective heat transfer to the fluid

Since there is incident solar energy on the absorber of the collector some portions of that will be transferred to the fluid by convection along the collector tube. This energy is called the useful energy and can be expressed as:

$$Q_u = A_p F_R [S_{\text{in}}(\tau\alpha) - U_T(T_{f,\text{in}} - T_a)] \quad (6)$$

In Eq. (6), T_p is replaced by fluid inlet temperature $T_{f,\text{in}}$ and the new term F_R which is heat removal factor is introduced and is found to be as below;

$$F_R = \frac{\dot{m} C_p}{A_p U_T} \left[1 - \exp\left(\frac{-A_p U_T F'}{\dot{m} C_p}\right) \right] \quad (7)$$

(F') is the collector efficiency factor and can be expressed as;

$$F' = \frac{(U_T)^{-1}}{W[U_T(D_o + (W - D_o)F)]^{-1} + (C_b)^{-1} + (\pi D_i h_f)^{-1}} \quad (8)$$

where C_b represents the bond conductance and it can be neglected ($1/C_b = 0$) as it is assumed to be very large.

And F is the fin efficiency is

$$F = \frac{\tanh[m(W - D_o/2)]}{m(W - D_o/2)}, \text{ where } m = \sqrt{\frac{U_T}{k\delta}} \quad (9)$$

In Eq. (8), h_f represents the convective heat transfer coefficient for both single and multi-phase conditions. The determination of heat transfer coefficient in single and multiphase flows is analysed in the following section.

3.2.1. Single-phase flow

For constant surface heat flux and fully developed single-phase laminar flow ($Re < 2300$) in a circular tube, Nusselt (Nu) number is constant and independent from Reynolds (Re) and Prandtl (Pr) numbers [27].

$$Nu = \frac{h_{sp} D}{k_{sp}} = 4.36 \quad (10)$$

For fully developed turbulent flow where $0.5 < Pr < 2000$ and $3 \times 10^3 < Re < 5 \times 10^6$ in a circular tube, Nusselt number can be obtained by Gnielinski equation which is a modification of Petukhov correlation [28].

$$Nu = \frac{\left(\frac{f}{8}\right)(Re - 1000)Pr}{1 + 12.7\left(\frac{f}{8}\right)^{0.5}(Pr^{2/3} - 1)} \quad (11)$$

3.2.2. Multiphase flow

A large number of theoretical and experimental studies have been conducted to calculate saturated flow boiling coefficient since it is important to reduce cost and gain better design of evaporators, boilers and other multiphase process components [29]. Among many studies a general and reliable correlation was investigated

by [30]. However, it was limited to vertical flows. Another correlation which is valid for both horizontal and vertical flows was generated by [31]. In this study, the chart correlation for the estimation of saturated boiling heat transfer coefficient that includes a comparison with 800 data points from 18 experimental studies is represented. Due to the difficulties of graphical form of correlations researchers have presented equations which express these chart correlations [32].

Following the Shah's method the procedure to calculate two-phase heat transfer coefficient is represented in this section. The correlations mainly consist of four dimensionless parameters in order to estimate heat transfer coefficient. The Froude number is given by the following equation [31];

$$Fr_1 = \frac{G^2}{\rho_1^2 g D_i} \quad (12)$$

Froude number is calculated to determine if the surface is fully wet or not. For vertical tubes the surface is fully wet independently of Froude number. However, for horizontal tubes if $Fr_1 > 0.04$ the surface is fully wet otherwise ($Fr_1 < 0.04$) the surface is partly dry. Once Froude number is determined then the dimensionless parameter N can be calculated for two different conditions;

3.2.3. Vertical and horizontal tubes

For vertical tubes at all conditions of Fr_1 values and for horizontal tubes when $Fr_1 > 0.04$ dimensionless parameter (N) equals to the convection number (Co).

3.2.4. Horizontal tubes

For horizontal tubes when $Fr_1 < 0.04$, then the following relation is applicable.

$$N = 0.38 Fr_1^{-0.3} Co \quad (13)$$

The next dimensionless parameter is the convection number (Co) and this can be calculated as [31];

$$Co = \left(\frac{1}{x} - 1\right)^{0.8} \left(\frac{\rho_g}{\rho_l}\right)^{0.5} \quad (14)$$

Another parameter is the enhancement factor (ψ) and it represents the ratio of multiphase flow heat transfer coefficient (h_{mp}) to the liquid phase heat transfer coefficient (h_l). Dittus-Boelter equation is used to calculate liquid phase heat transfer coefficient in this analysis [31].

Then, the calculation is followed by the evaluation of both nucleate and convective boiling factor. For the calculation of nucleate boiling factor three applicability conditions of the dimensionless number (N) are represented below [33];

For $N > 1$

$$\psi_{\text{nb}} = 230 Bo^{0.5} \quad \text{If } Bo > 0.3 \times 10^{-4}$$

$$\psi_{\text{nb}} = 1 + 46 Bo^{0.5} \quad \text{If } Bo < 0.3 \times 10^{-4}$$

ψ_{nb} and Bo represents nucleate boiling factor and boiling number respectively. Bo is calculated as [31];

$$Bo = \frac{\Phi}{GH_{\text{fg}}} \quad (15)$$

where Φ is the heat flux, G is the mass flux and H_{fg} represents heat of vaporization.

Convective boiling factor ψ_{cb} is given by the following Eq. (16).

$$\psi_{\text{cb}} = 1.8 N^{-0.8} \quad (16)$$

As both nucleate boiling factor ψ_{nb} and convective boiling factor ψ_{cb} are calculated, the larger value is taken as enhancement factor and is used to calculate multi phase heat transfer coefficient (h_{mp}).

For $0.1 < N < 1$

$$\psi_{nb} = FBo^{0.5} \exp(2.74N^{-0.1}) \quad (17)$$

ψ_{cb} is determined from Eq. (16) and ψ equals to the larger value of ψ_{nb} or ψ_{cb} .

For $N < 0.1$

$$\psi_{nb} = FBo^{0.5} \exp(2.47N^{-0.15}) \quad (18)$$

ψ_{cb} is evaluated from Eq. (16) and ψ equals to the larger value of ψ_{nb} or ψ_{cb} .

The constant F is as follows [33];

$Bo > 0.0011$, $F = 14.7$.

$Bo < 0.0011$, $F = 15.43$.

4. Iteration procedure

During the research a numerical model is developed to simulate flat plate collector performance, fluid temperature and heat transfer coefficient along the tube. Collector specifications and operating parameters are shown in Tables 1 and 2.

Basically, the model relies on dividing the collector tube into small finite elements and calculating the fluid outlet temperature, plate temperature, the heat loss coefficient, the useful heat, the heat gain and the enthalpy values iteratively. As shown in Fig. 2 for each element the outlet temperature and enthalpy values are set equal to the inlet conditions of the next element till the end of the last element.

Initially, the model starts with calculating the heat loss coefficient by using Eq. (1). As it can be seen from Eq. (1) plate temperature (T_p) is necessary to determine the heat loss coefficient (U_T). Since T_p is an unknown an arbitrary value which is estimated as 5 °C higher than inlet fluid temperature is given in order to calculate U_T . Then, the model evaluates useful heat (Q_u) by introducing the calculated U_T into Eq. (6). In order to determine heat transfer coefficient, the fluid flow is defined whether it is laminar or turbulence by calculating Reynolds (Re) number. Depending on the flow type, Nusselt (Nu) number is determined and heat transfer coefficient is calculated by using Eqs. (10) and (11). Fluid thermodynamic properties such as saturation temperature (T_{sat}),

thermal conductivity (k), density (ρ), specific heat (C_p), viscosity (μ) and enthalpy (H) are calculated by developed regression equations. Data for the regression analysis is taken from REFPROP 9.1 programme [34] for various temperature values. Desired properties of the fluid are estimated by introducing fluid mean temperature into the regression equations. The estimated plate temperature is used to determine initial fluid mean temperature as the outlet temperature of the fluid is not known. Initial fluid mean temperature is defined as;

$$T_{f,m} = \frac{T_p + T_{f,in}}{2} \quad (19)$$

However, calculated Q_u represents the amount of useful heat for the whole collector tube. This can be represented by Eq. (20).

$$Q_u = Q_u'' \pi D_{in} L_{tube} \quad (20)$$

where Q_u'' is the useful heat rate and πD_{in} is the surface perimeter. In other words, the useful heat rate can be obtained by dividing useful heat (Q_u) by the surface area of the collector ($\pi D_{in} L_{tube}$). To calculate heat gain for each small element the rate of useful heat is multiplied by the surface perimeter and the length of each element which is defined previously by dividing total collector length into small finite elements. Therefore, heat gain of each element can be evaluated by;

$$Q_{gain} = Q_u'' \pi D_{in} \int_0^L dx \quad (21)$$

Once the heat gain is evaluated for the first element the fluid outlet temperature is calculated by introducing Q_{gain} into Eq. (22).

$$T_{f,out} = T_{f,in} + \frac{Q_{gain}}{\dot{m} C_p} \quad (22)$$

Calculated fluid outlet temperature $T_{f,out}$ is introduced into Eq. (23) to determine new fluid mean temperature. The new mean fluid temperature can be determined as;

$$T_{f,m} = \frac{T_{f,in} + T_{f,out}}{2} \quad (23)$$

The new mean temperature calculated by Eq. (23), is used for determining the new Q_u . After calculating the new Q_u , a new plate temperature is calculated as;

$$T_p = T_{f,in} + \frac{Q_u/A_p}{F_R U_T} (1 - F_R) \quad (24)$$

Then, the algorithm re-evaluates U_T , Q_u and Q_{gain} by utilizing the new plate temperature and the new fluid mean temperature in Eqs. (3), (6) and (21). This process is repeated in the first loop until the difference between T_p and its value in the previous iteration and T_{out} and its value in the previous iteration is lower than convergence criteria. Convergence criterion of 0.01 °C was selected for the iterated indicators mentioned above and the results converge within 10 iterations.

Second loop checks if the outlet temperature of the element reaches the saturation temperature of the fluid at corresponding pressure. If the exit temperature does not provide saturation conditions then algorithm increases the number of element. In other words, the length of the tube is increased and the same calculations are performed for the next element. Once the outlet temperature reaches the saturation temperature then flow boiling occurs in the collector tube. In the flow boiling calculations same steps are followed with the exception of calculating single phase heat transfer coefficient, multiphase heat transfer coefficient is calculated. Since the fluid temperature is constant in boiling outlet enthalpy is determined as;

$$H_{f,out} = H_{f,in} + \frac{Q_{gain}}{\dot{m}} \quad (25)$$

Table 1
Collector specifications.

Collector area (m ²)	6.96
Absorber plate thermal conductivity (W/m K)	50
Absorber plate thickness (m)	0.001
Total length of tube (m)	56
Tube inner diameter (m)	0.008
Tube outer diameter (m)	0.01
Effective transmittance-absorbance product (-)	0.81

Table 2
System parameters.

Fluid inlet temperature (K)	278
Fluid mass flow rate (kg/s)	0.001–0.005–0.01
Ambient temperature (K)	275
Operating pressure (bar)	4–6–8
Incoming solar radiation (W/m ²)	500
Wind velocity (m/s)	2

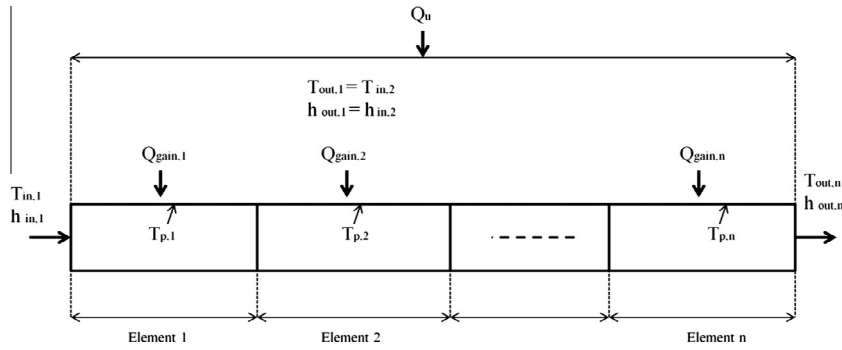


Fig. 2. Schematic of collector elements.

In boiling region vapour quality of the fluid is calculated at each element using Eq. (26).

$$x = \frac{H_{f,out} - H_l}{H_g - H_l} \quad (26)$$

where H_l and H_g represent saturated liquid and saturated vapour enthalpy of the fluid, respectively. The third loop also checks if the vapour quality reaches 1 at the end of each element. Multiphase flow calculations continue with the increase of elements since the fluid become superheated vapour ($x > 1$). At this point same calculations are performed with the single phase heat transfer coefficient which was mentioned above. The only difference is superheated

vapour properties of the fluid are determined and used in the calculations.

A computer code is developed via Matlab software to perform iterative computations. Flowchart of the computer code is represented in Fig. 3.

5. Results and discussion

The simulation study is conducted with HFC-134a and its transport and thermodynamic properties can be found in [34]. Fig. 4 shows that the fluid enters to the collector at 5 °C temperature and 6 bar pressure. Its mean temperature increases along the col-

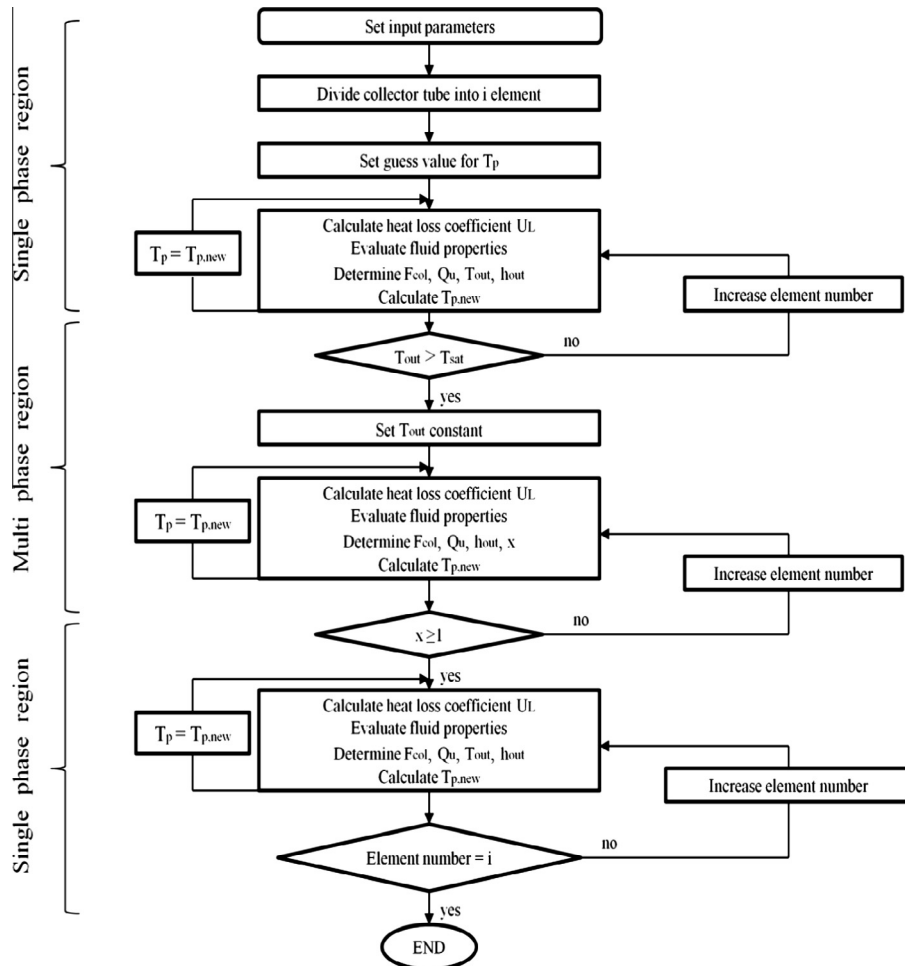


Fig. 3. Flow chart of the simulation study.

lector tube as the useful heat gain of the fluid raises. The increment in fluid mean temperature continues until it reaches the corresponding boiling temperature (22.2 °C). This region is called liquid single-phase flow which corresponds to 29% of total length of the collector tube. If the fluid reaches its saturation point, the fluid mean temperature remains constant and the fluid undergoes a phase-change. The region where saturated liquid turns into saturated vapour indicates multiphase flow or flow boiling. Boiling region occupies 58% of the tube. The heat gain of the fluid also increases during the flow boiling and this heat is used to generate vapour in the tube. Once the liquid completely turns into saturated vapour where the vapour quality equals to 1 represents the end of the boiling region. As the fluid continues gaining the heat its temperature increases again along the collector tube. This region is called vapour single-phase flow in which saturated vapour turns into superheated vapour. This phenomena proceeds till the end of the collector tube. The fluid temperature reaches 26.3 °C at the end of the tube and leaves the collector as a superheated vapour.

Fig. 5 represents the convective heat transfer coefficient of HFC-134a in both single-phase (liquid and vapour) and multiphase flows. In the liquid single phase region, the heat transfer coefficient ranged from 153.54 W/m² K to 173.93 W/m² K where as it changed from 375.2 W/m² K to 416.66 W/m² K in multiphase region. This indicates that in flow boiling the heat transfer coefficient is considerably higher than in single-phase region. Fig. 5 is generally in agreement with the studies [11,12]. In superheated vapour region, the heat transfer coefficient decreased to 73.4 W/m² K and remained almost constant.

The variation of flow boiling heat transfer coefficient versus vapour quality is shown in Fig. 6. Heat transfer coefficient increases

from 375.2 W/m² K to 498.23 W/m² K as the vapour quality increases. The maximum heat transfer coefficient (610.27 W/m² K) is observed at a quality of $x = 0.8$ then it decreased gradually to 498.23 W/m² K.

This could be explained by the occurrence of dry out which results in a decrease in the heat transfer coefficient due to the low conductivity of dry steam [35]. Fig. 7 indicates that at constant pressure (6 bars), liquid single phase heat transfer coefficient and useful heat gain of the fluid increases with the increasing mass flow rate.

As the mass flow rate increases from 0.001 kg/s to 0.01 kg/s heat transfer coefficient and heat gain of the fluid increases from 39.24 W/m² K to 392.31 W/m² K and from 61.17 W to 535.13 W respectively. An increase in mass flow rate yields to a rise in Reynolds number, in other words a transition from laminar flow to turbulent flow in collector tubes. This results in a greater value of heat transfer coefficient and more heat which transferred to the working fluid. Instead of conventional fluid temperature absorber temperature is considered to develop efficiency equation for the collector. Collector efficiency η_{col} can be determined as follows:

$$\eta_{col} = \frac{Q_p}{S_{in}A_p} = \frac{A_p [S_{in}(\tau\alpha) - U_T(T_p - T_a)]}{S_{in}A_p} \quad (27)$$

It can be seen from Fig. 8 that the collector efficiency increases from 60.2% to 68.8% while absorber plate temperature decreases from 45.53 °C to 29.7 °C. This phenomenon indicates that the more heat is gained by the fluid the more heat which is absorbed on the absorber plate is transferred to the fluid. Increase in heat transfer from the absorber plate to the working fluid yields to a decrease

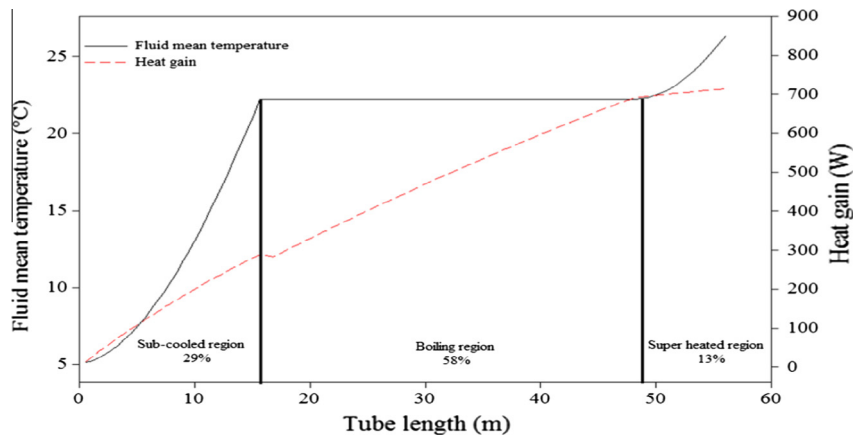


Fig. 4. Fluid mean temperature and heat gain variation along the collector tube ($P = 6$ bar, $m = 0.005$ kg/s).

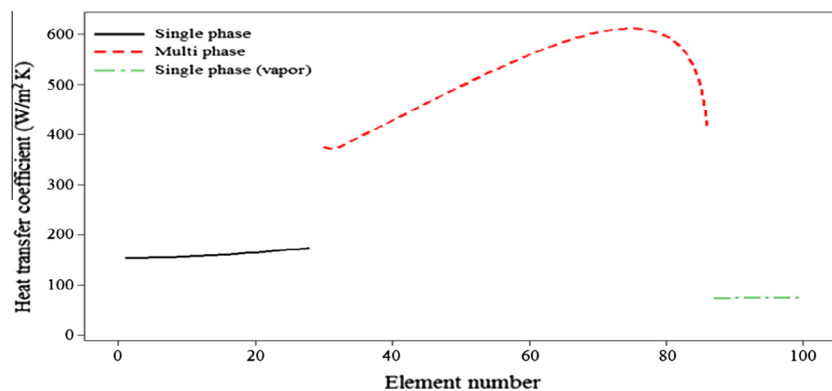


Fig. 5. Fluid heat transfer coefficient in various flow regions ($P = 6$ bar, $m = 0.005$ kg/s).

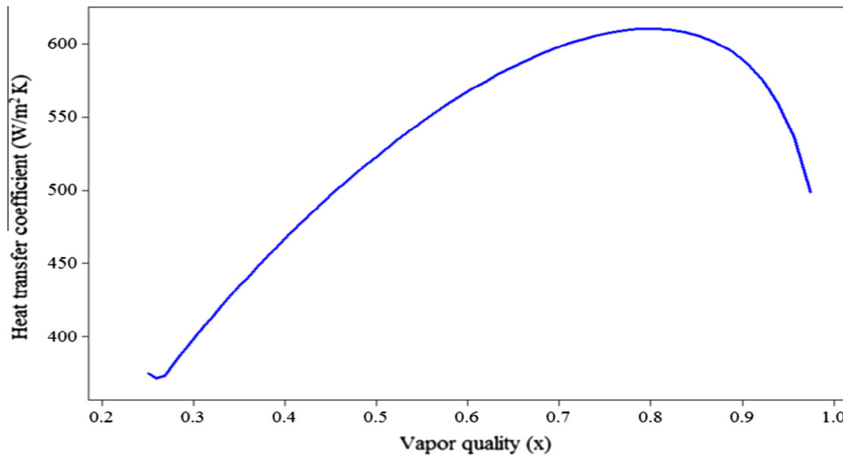


Fig. 6. Boiling heat transfer coefficient versus vapour quality ($P = 6$ bar, $m = 0.005$ kg/s).

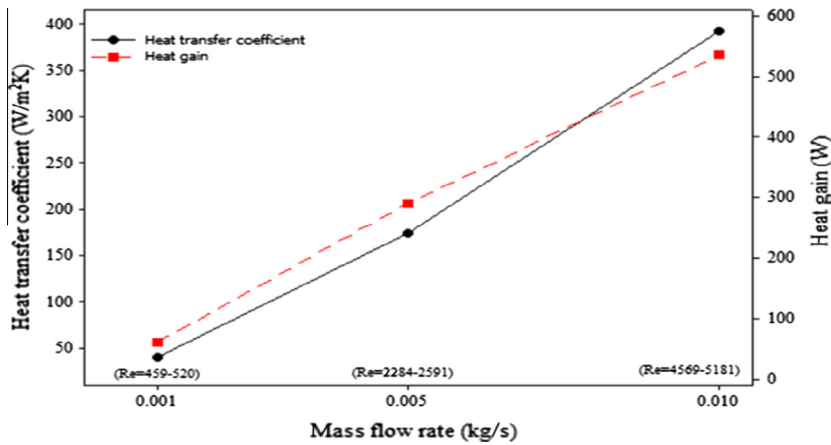


Fig. 7. Heat transfer coefficient and heat gain at various mass flow rates ($P = 6$ bar).

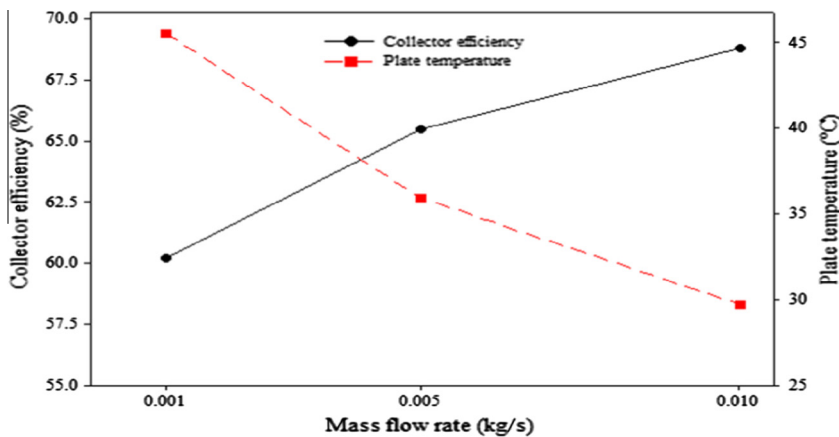


Fig. 8. Collector efficiency and plate temperature at various mass flow rates ($P = 6$ bar).

in the absorber plate temperature which brings less heat loss from the collector plate to the surroundings. As a result higher collector efficiency value is observed.

Fig. 9 represents the effect of inlet pressure of the fluid on the plate temperature and collector efficiency at constant mass flow rate ($\dot{m} = 0.005$ kg/s).

It can be seen from Fig. 9 that saturation temperature increases from 9.6 °C to 31.9 °C as the operating pressure of the collector increases from 4 bars to 8 bars. At saturation temperature of 9.6 °C plate temperature is found 22.1 °C whereas plate temperature is found 41.8 °C at 31.9 °C saturation temperature. Moreover, a decrease in the collector efficiency from 72.5% to 62.3% is due

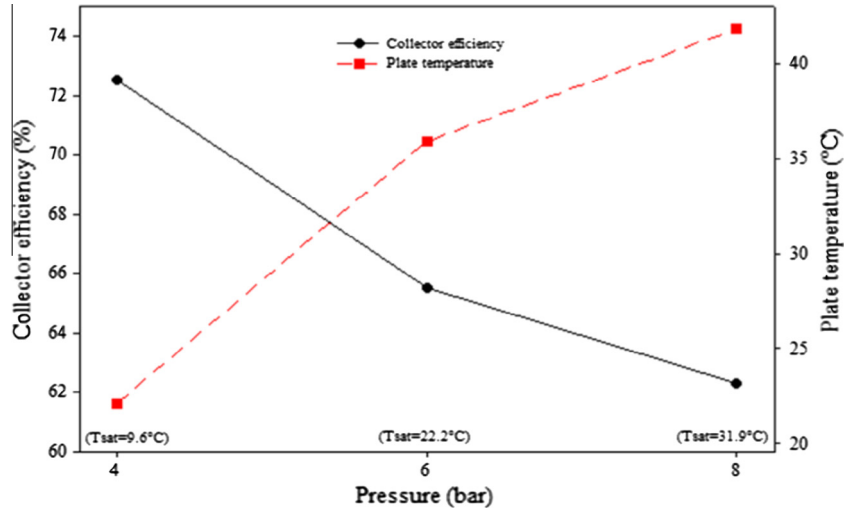


Fig. 9. Collector efficiency and plate temperature at various operating pressure ($m = 0.005$ kg/s).

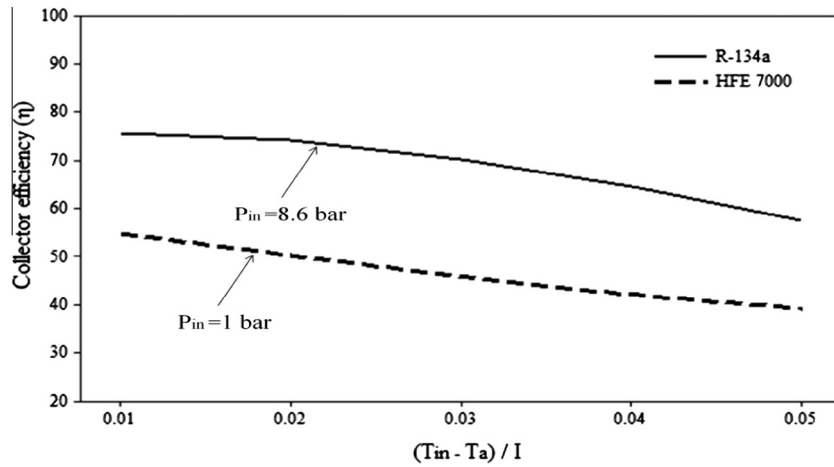


Fig. 10. Collector efficiency as a function of $(T_{in} - T_a) / I$ with R-134a and HFE-7000 for the same saturation temperature condition.

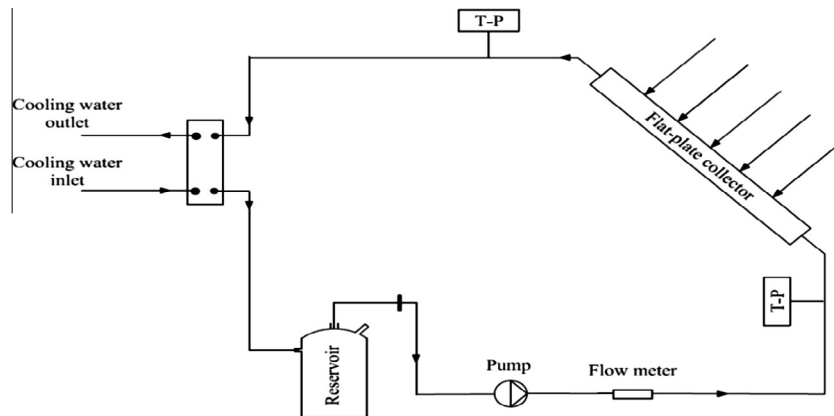


Fig. 11. Schematic of the experimental test rig.

to the increase in the plate temperature and thus causes thermal loss from the collector.

In Fig. 10 the efficiency of the flat-plate collector using both R-134a and HFE-7000 versus reduced temperature $(T_{in} - T_a) / I$ is represented. In the analysis fluid saturation temperature for both

fluids are 15 °C higher than the fluid inlet temperature at corresponding collector operating pressures. As it can be seen from Fig. 10 that for the same incident radiation ($I = 500$ W/m²), mass flow rate ($\dot{m} = 0.005$ kg/s) and inlet temperature (20 °C) R-134a gives higher collector performance than HFE-7000 in both

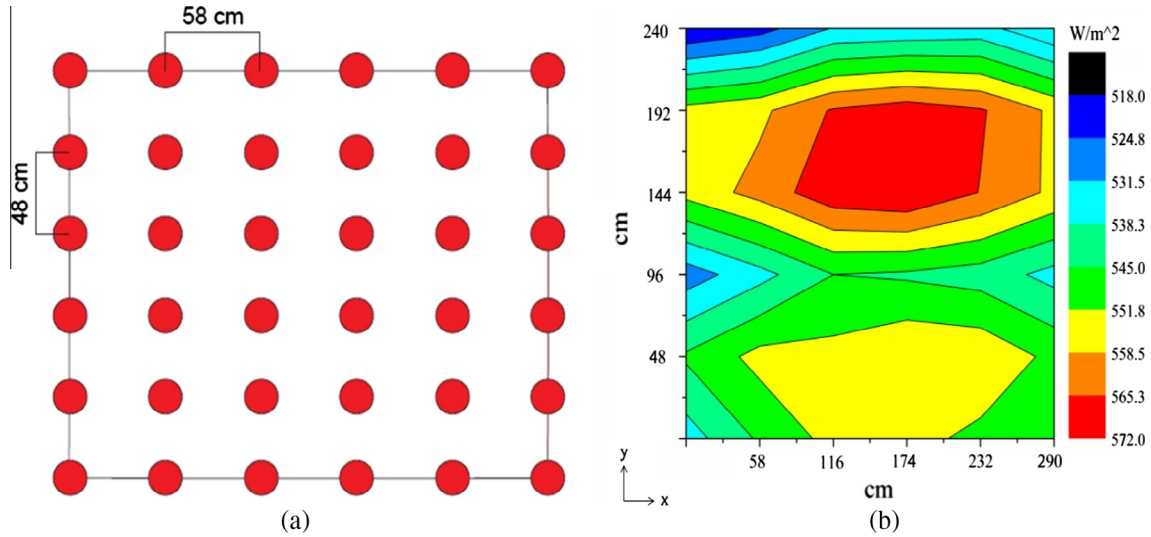


Fig. 12. (a) Measured points on the collector surface and (b) solar radiation distribution on the collector surface.

Table 3
Experimental conditions.

Parameter	Unit	Value
Collector inlet temperature	°C	28.4–47.9
Ambient temperature	°C	18
Collector inlet pressure	bar	1.4–2.1
Fluid mass flow rate	kg/s	0.012–0.013
Solar radiation	W/m ²	550

non-boiling and boiling region. This could be explained by relatively higher thermal conductivity of R-134a ($k = 0.083 \text{ W/m K}$) than HFE-7000 ($k = 0.0757 \text{ W/m K}$) at given conditions.

6. Experimental validation

In order to validate the proposed mathematical and numerical models an experimental test rig was designed and commissioned. The test rig consists of a flat plate collector, a circulation pump, a reservoir and a heat exchanger (Fig. 11).

The flat plate collector specifications are given in Table 1 previously. A solar simulator was employed as an artificial source of radiation to provide steady radiant energy to the collector. Solar simulator consists of 12 glare lamps and each lamp can provide 1 kW heat output. In the experiments 6 kW heat is supplied from

the simulator to the collector. A pyranometer (Kipp&Zonen CMP3) was used to measure the irradiance on the collector surface. The solar simulator placed 2 m away from the collector surface during the measurements. Fig. 12(a) shows the measured points on the collector surface. It is found that the distributed heat flux ranged from 518 to 572 W/m² on the collector surface and the average irradiance over the collector surface ($2.9 \times 2.4 \text{ m}$) is 550 W/m² (Fig. 12(b)).

Although HFC 134a was used in the simulation study, in order to check the compatibility of the mathematical and the numerical models a novel working thermo-fluid (HFE 7000) was utilized in the experiment. The new simulation study using HFE 7000 was conducted and the fluid outlet temperature of the simulation was compared with the experimental data. The required thermodynamic and transport properties of HFE 7000 were taken from REFPROP 9.1 programme. Furthermore, HFE 7000 has a higher boiling point temperature (34 °C at 1 atm) than HFC 134a (−26 °C at 1 atm) and therefore it is easier to handle at atmospheric conditions. Initially 8 kg of HFE 7000 was charged in the system and it was compressed by the pump and sent to the collector. The absorbed heat which is converted from simulated solar radiation in the collector is transferred to the fluid via convective heat transfer mechanism. The fluid exits the collector with a higher temperature and reaches the heat exchanger. Some portion of its

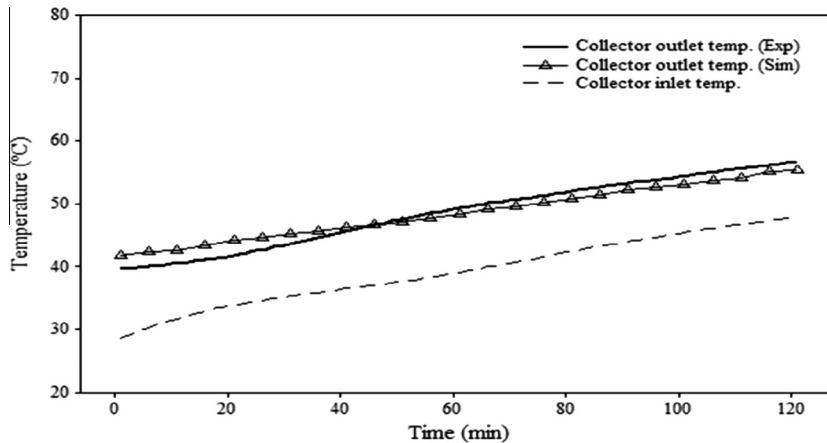


Fig. 13. Fluid temperatures at the inlet and outlet of the collector.

Table A.1
Measured parameters and their uncertainties.

Instruments	Measured parameters	Range	Uncertainty (%)
Thermocouples (°C)	Collector inlet temperature	0–100 (°C)	2.5
	Collector outlet temperature	0–100 (°C)	2
Pressure transmitters (bar)	Collector inlet pressure	0–10 (bar)	3.0
	Collector outlet pressure	0–10 (bar)	3.5
Flow meter (l/min)	Fluid flow rate	0.12–1.6 (l/min)	3.2

heat is rejected from the system and therefore its temperature decreases in the heat exchanger. Tap water is used to cool and condense the working fluid. The fluid is collected in the reservoir and is then compressed by the pump again to complete the cycle.

In order to measure temperature and pressure values of the fluid, K-type thermocouples with an accuracy of $\pm 0.18\%$ and pressure transmitters with an accuracy of $\pm 0.5\%$ are mounted at the inlet and outlet of the collector. A flow meter is placed 65 cm away from the pump to measure the volumetric flow rate of the fluid and the accuracy of the flow meter is $\pm 2\%$. Temperature, pressure and flow rate data of the fluid are recorded and transmitted to a computer by a data acquisition unit. Table 3 represents the environmental and the inlet conditions of the experiment.

It can be seen from Fig. 13 that the model can predict the outlet temperature of the fluid with a small range of deviation. The deviation for the outlet temperature of the fluid between the simulation and the experimental results ranged from 0.45% to 4.9%.

7. Conclusions

A numerical model for the flat plate collector was developed to simulate the collector performance under various conditions. The derived algorithm can solve the model and can iteratively evaluate the fluid mean temperature, fluid heat gain, absorber temperature and the heat transfer coefficient of the fluid at any point along the flow direction. The model is capable of calculating single phase heat transfer coefficient, as well as the multiphase heat transfer coefficient of the fluid if its temperature surpasses its boiling temperature in the collector. The algorithm was implemented by utilizing the MATLAB programme. The model was solved with HFC-134a refrigerant. The simulation results showed that in the flow boiling region the heat transfer coefficient ($375.2\text{--}416.6\text{ W/m}^2$) is higher than in single phase liquid ($153.54\text{--}173.93\text{ W/m}^2$) and single phase vapour (73.4 W/m^2) regions. Effect of the mass flow rate and the pressure on the heat transfer coefficient, collector efficiency and heat gain of the fluid is also taken into account in the simulation study. It is found that heat transfer coefficient have shown a dependency on the flow rate of the flow. As the mass flow rate, as well as the Reynolds number of the flow increases, the flow becomes turbulent. In turbulent region higher heat transfer coefficient is obtained than laminar region which leads to an increase in the heat gain of the fluid and the efficiency of the collector. Analysis of the simulation results also showed that operating pressure, in other words saturation pressure of the fluid has an effect on the collector efficiency. In higher saturation pressure condition in the collector saturation temperature becomes further from the inlet fluid temperature and the efficiency of the collector decreases. Furthermore, the collector efficiency with two working fluids (R-134a and HFE-7000) is compared for the same inlet conditions. It is found that R-134a gives higher collector efficiency due to its superior properties compared to the HFE-7000 at given conditions. An experimental test rig was built in order to validate the simulation model against experimental results. HFE-7000 was utilized in the experiment and the simulation results for HFE-7000 show good agreement with the experimental results.

Acknowledgment

This research is funded by Future Energy Source (FES) Ltd, UK. The authors acknowledge in-kind support provided by Mr Brian Camfield and Mr Tony Camfield.

Appendix A. Uncertainty analysis

In order to evaluate the accuracy and the reliability of the measured parameters an uncertainty analysis is conducted. The measured instruments and their uncertainties are shown in Table A.1.

References

- [1] Baharoon DA, Rahman HA, Omar WZW, Fadhil SO. Historical development of concentrating solar power technologies to generate clean electricity efficiently – a review. *Renew Sustain Energy Rev* 2015;41:996–1027.
- [2] Villicana-Ortiz E, Gutierrez-Trashorras AJ, Paredes-Sanchez JP, Xiberta-Bernat J. Solar energy potential in the coastal zone of the Gulf of Mexico. *Renewable Energy* 2015;81:534–42.
- [3] Bozkurt I, Karakilcik M. The effect of sunny area ratios on the thermal performance of solar ponds. *Energy Convers Manage* 2015;91:323–32.
- [4] Owrak M, Aminy M, Jamal-Abad MT, Dehghan M. Experiments and simulations on the thermal performance of a sunspace attached to a room including heat-storing porous bed and water tanks. *Build Environ* 2015;92:142–51.
- [5] Chen X, Xia XL, Meng X-L, Dong X-H. Thermal performance analysis on a volumetric solar receiver with double-layer ceramic foam. *Energy Convers Manage* 2015;97:282–9.
- [6] Dehghan M, Rahmani Y, Ganji DD, Saedodin S, Valipour MS, Rashidi S. Convection–radiation heat transfer in solar heat exchangers filled with a porous medium: Homotopy perturbation method versus numerical analysis. *Renewable Energy* 2015;74:448–55.
- [7] Dehghan M, Mahmoudi Y, Valipour MS, Saedodin S. Combined conduction–convection–radiation heat transfer of slip flow inside a micro-channel filled with a porous material. *Transp Porous Media* 2015;108:413–36.
- [8] Kalogirou SA. Solar thermal collectors and applications. *Prog Energy Combust Sci* 2004;30:231–95.
- [9] Zamzamin A, Keyanpourrad M, Kianineyestani M, Jamal-Abad MT. An experimental study on the effect of Cu-synthesized/EG nanofluid on the efficiency of flat-plate solar collectors. *Renewable Energy* 2014;71:658–64.
- [10] Colangelo G, Favale E, Miglietta P, De Risi A, Milanese M, Laforgia D. Experimental test of an innovative high concentration nanofluid solar collector. *Appl Energy* 2015;154:874–81.
- [11] Abramzon B, Yaron I, Borde I. An analysis of a flat-plate solar collector with internal boiling. *J Sol Energy Eng* 1983;105:454–60.
- [12] Price H, Klein S, Beckman W. Analysis of boiling flat-plate collectors. *J Sol Energy Eng* 1986;108:150–7.
- [13] Zhang X-R, Yamaguchi H, Umeno D. Experimental study on the performance of solar Rankine system using supercritical CO₂. *Renewable Energy* 2007;32:2617–28.
- [14] Marion M, Voicu I, Tiffonnet A-L. Study and optimization of a solar subcritical organic Rankine cycle. *Renewable Energy* 2012;48:100–9.
- [15] Delgado-Torres AM, García-Rodríguez L. Analysis and optimization of the low-temperature solar organic Rankine cycle (ORC). *Energy Convers Manage* 2010;51:2846–56.
- [16] Wang J, Zhao L, Wang X. A comparative study of pure and zeotropic mixtures in low-temperature solar Rankine cycle. *Appl Energy* 2010;87:3366–73.
- [17] Wang X, Zhao L, Wang J, Zhang W, Zhao X, Wu W. Performance evaluation of a low-temperature solar Rankine cycle system utilizing R245fa. *Sol Energy* 2010;84:353–64.
- [18] Gorozabel Chata FB, Chaturvedi SK, Almogbel A. Analysis of a direct expansion solar assisted heat pump using different refrigerants. *Energy Convers Manage* 2005;46:2614–24.
- [19] Zhang D, Wu QB, Li JP, Kong XQ. Effects of refrigerant charge and structural parameters on the performance of a direct-expansion solar-assisted heat pump system. *Appl Therm Eng* 2014;73:522–8.

- [20] Chaturvedi SK, Gagrani VD, Abdel-Salam TM. Solar-assisted heat pump – a sustainable system for low-temperature water heating applications. *Energy Convers Manage* 2014;77:550–7.
- [21] Chow TT, Pei G, Fong KF, Lin Z, Chan ALS, He M. Modeling and application of direct-expansion solar-assisted heat pump for water heating in subtropical Hong Kong. *Appl Energy* 2010;87:643–9.
- [22] Aziz W, Chaturvedi S, Kheireddine A. Thermodynamic analysis of two-component, two-phase flow in solar collectors with application to a direct-expansion solar-assisted heat pump. *Energy* 1999;24:247–59.
- [23] Khan ZA, Hadfield M, Tobe S, Wang Y. Ceramic rolling elements with ring crack defects – a residual stress approach. *Mater Sci Eng, A* 2005;404:221–6.
- [24] Khan ZA, Hadfield M, Wang Y. Pressurised chamber design for conducting rolling contact experiments with liquid refrigerant lubrication. *Mater Des* 2005;26:680–9.
- [25] Duffie JA, Beckman WA. *Solar engineering of thermal processes*. John Wiley & Sons; 2013.
- [26] Klein S. Calculation of flat-plate collector loss coefficients. *Sol Energy* 1975;17:79–80.
- [27] Cengel Y. *Heat transfer: a practical approach*. Columbus, OH: McGraw Hill; 2003.
- [28] Incropera FP. *Fundamentals of heat and mass transfer*. John Wiley & Sons; 2011.
- [29] Kandlikar SG. A general correlation for saturated two-phase flow boiling heat transfer inside horizontal and vertical tubes. *J Heat Transfer* 1990;112:219–28.
- [30] Chen JC. Correlation for boiling heat transfer to saturated fluids in convective flow. *Ind Eng Chem Process Des Dev* 1966;5:322–9.
- [31] Shah MM. A new correlation for heat transfer during boiling flow through pipes. *Ashrae Trans* 1976;82:66–86.
- [32] Shah M. *Chart correlation for saturated boiling heat transfer: equations and further study*. 1982.
- [33] Collier JG, Thome JR. *Convective boiling and condensation*. Oxford University Press; 1994.
- [34] Lemmon E, Huber M, McLinden M. N. REFPROP. Standard reference database 23. REFPROP, NIST, Version. 9.1; 2013.
- [35] Odeh S, Morrison G, Behnia M. Modelling of parabolic trough direct steam generation solar collectors. *Sol Energy* 1998;62:395–406.